TU Delft

Delft University of Technology

Document Version
Final published version

Licence
CC BY

Citation (APA)
Wang, C., de Vries, L. J., van de Pas, V., Werner, S., De Wagter, C., & Muijres, F. T. (2026). Visual-inertial integration enables bumblebees to land on rapidly moving flowers. *Journal of the Royal Society, Interface*, *23*(242), Article 20251198. https://doi.org/10.1098/rsif.2025.1198

Important note
To cite this publication, please use the final published version (if applicable).
Please check the document version above.

Copyright
In case the licence states “Dutch Copyright Act (Article 25fa)”, this publication was made available Green Open Access via the TU Delft Institutional Repository pursuant to Dutch Copyright Act (Article 25fa, the Taverne amendment). This provision does not affect copyright ownership.
Unless copyright is transferred by contract or statute, it remains with the copyright holder.

Sharing and reuse
Other than for strictly personal use, it is not permitted to download, forward or distribute the text or part of it, without the consent of the author(s) and/or copyright holder(s), unless the work is under an open content license such as Creative Commons.

Takedown policy
Please contact us and provide details if you believe this document breaches copyrights.
We will remove access to the work immediately and investigate your claim.

This work is downloaded from Delft University of Technology.

INTERFACE

royalsocietypublishing.org/rsif

CC BY

Research

Cite this article: Wang C, de Vries LJ, van de Pas V, Werner S, De Wagter C, Muijres FT. 2026 Visual–inertial integration enables bumblebees to land on rapidly moving flowers. *J. R. Soc. Interface* **23**: 20251198.
https://doi.org/10.1098/rsif.2025.1198

Received: 21 November 2025
Accepted: 25 June 2026

Subject Category:
Life Sciences–Physics interface

Subject Areas:
biomechanics, biomimetics

Keywords:
insect flight control, landing dynamics, bio-inspired robotics, control theory

Author for correspondence:
Florian T. Muijres
e-mail: florian.muijres@wur.nl

Supplementary material is available online at https://doi.org/10.6084/m9.figshare.c.8583027.

THE ROYAL SOCIETY PUBLISHING

Visual–inertial integration enables bumblebees to land on rapidly moving flowers

Chenyao Wang[1], Lana J. de Vries[1], Vincent van de Pas[1], Steffen Werner[1], Christophe De Wagter[2] and Florian T. Muijres[1]

[1]Experimental Zoology Group, Wageningen University, Wageningen, The Netherlands
[2]Micro Air Vehicle Laboratory, Delft University of Technology, Delft, The Netherlands

CW, 0009-0001-1493-5355; FTM, 0000-0002-5668-0653

Landing on a moving target is challenging for flying animals, particularly under dynamic outdoor conditions. For pollinators such as bumblebees, wind-induced flower motion adds substantial complexity to landing manoeuvres. Here, we investigate how bumblebees (*Bombus terrestris*) land on laterally oscillating flowers. Using high-speed stereoscopic videography, we quantified three-dimensional flight kinematics of 48 bumblebees approaching a sinusoidally moving flower-mimic and analysed their control strategies using system-identification and control-theoretic modelling. Landing dynamics were consistent with combined visual (optic-flow) and angular yaw-rate feedback, enabling precise sideways tracking and gaze stabilization. Sideways motion was captured by a proportional controller, whereas gaze control required a proportional–derivative structure. Both controllers yielded similar case-specific effective delays (approximately 54 and 52 ms). Surprisingly, optic-target-angle contributed negligibly to gaze control, indicating reliance on velocity-based rather than position-based cues. Lateral acceleration correlated strongly with body roll, consistent with the helicopter model of force redirection. These results reveal a modular visual–inertial control strategy enabling robust landings on moving targets and suggest principles for agile bio-inspired flight.

1. Introduction

Landing precisely on targets is important for all flying animals, particularly insect pollinators that must repeatedly touch down on flowers. However, in natural environments, gusts introduce airflow perturbations that affect the kinematics of both pollinators and flowers [1,2].

For a successful touchdown, bees rely primarily on visual cues [3], using optic-flow (OF) [1,4], optic-expansion [3,5] and optic-target-angle (OTA) [1,6] to estimate relative position and velocity. As a velocity-based signal, OF quantifies the apparent motion of objects across the observer's view [4]. Optic-expansion provides a cue for estimating approach speed by measuring an object's image enlargement rate, i.e. the divergence of the OF field [7]. The OTA, in turn, provides a position-based cue defined by the target's viewing angle.

The visual–motor control system of bees has been extensively studied across flight scenarios. During free flight, bees regulate speed using global OF [8]. When landing on vertical surfaces, bees use optic-expansion to control approach speed [3,5], maintaining a near-constant expansion for linear deceleration [3]. However, this strategy can cause oscillations near targets [9], which bees mitigate through a stepwise constant optic-expansion strategy [5].

Most previous work has focused on longitudinal kinematics during approaches to stationary targets, whereas lateral control during landings on

© 2026 The Authors. Published by the Royal Society under the terms of the Creative Commons Attribution License http://creativecommons.org/licenses/by/4.0/, which permits unrestricted use, provided the original author and source are credited

Downloaded from royalsocietypublishing.org/rsif/article-pdf/doi/10.1098/rsif.2025.1198/6167060/rsif.2025.1198.pdf
by guest
on 30 September 2026

moving targets remains less explored. Honeybees can track and land on horizontally moving targets using target angular velocity and OTA [6]. Similarly, bumblebees follow pseudo-randomly moving targets while stabilizing gaze by minimizing sideways OF and OTA during landing [1]. By contrast, studies on fruitflies suggest that apparent positional centring may arise from motion-dependent control, where velocity-based optomotor responses and integrated movement cues dominate tracking rather than explicit retinal position signals [10–12].

In addition to visual cues, bees also rely on inertial feedback. Bees integrate visual and inertial signals to counter wind perturbations when flying [13]. This feedback is likely mediated by mechanoreceptors on the antennae [14] and wings [15], including campaniform sensilla [15]. In Diptera, halteres act as specialized gyroscopic organs [16]; Hymenoptera lack such structures, and no dedicated inertial sensor has been conclusively identified. However, wing deformation during body rotations may provide rotation-related feedback via campaniform sensilla [17]. Importantly, angular rate could be derived from visual motion cues alone [18]. In the present study, yaw rate is therefore treated as a task-relevant state variable within a phenomenological control framework, without implying the existence of a specialized gyroscopic organ in bees.

In summary, while approach speed control during landings on stationary targets is extensively studied and modelled, the sensory–motor feedback mechanisms underlying sideways control during landings on moving targets remain poorly understood. To address this, we studied how bumblebees (*Bombus terrestris*) control lateral motion when landing on moving flowers. We hypothesized that bumblebees use both visual and inertial sensory feedback to regulate sideways movements and gaze. Bumblebees were trained to land on a sinusoidally moving flower-mimic, and their trajectories were recorded with high-speed cameras. Lateral kinematics were then decoupled from longitudinal motion, and decomposed into translational sideway-following to align with flower motion, and rotational yaw-steering to maintain gaze on the flower.

Understanding such multi-modal control strategies requires a quantitative framework, well suited to control theory. Control theory has been widely applied to model dynamics and estimate parameters in flying insects and their bio-inspired robotic counterparts, flapping-wing micro-aerial vehicles (FWMAVs) [14,19–22].

In fruitflies, control-theoretic models have elucidated flight control mechanisms, including integrative sensory-feedback regulation of flight dynamics [23] and combined visual–inertial control of manoeuvres [14,19]. Rotational kinematics were modelled through analyses of rapid corrective manoeuvres [24–27]. Fruitfly yaw dynamics follow a proportional–derivative (PD) feedback model incorporating passive flapping damping [24,25], whereas gaze control is likewise PD-based with separate head and body pathways [20]. Proportional–integral (PI) models efficiently capture pitch [26] and roll [27] corrections in fruitflies. Similar PD models also captured bumblebee flight stabilization. A simplified six-degree-of-freedom dynamics model demonstrated that a three-axis PD controller effectively stabilizes hovering [21]. In FWMAVs, proportional–integral–derivative (PID) control enhances stability and gust adaptation through adaptive feed-forward and gain-scheduling [22]. Beyond PID control, other modelling approaches further demonstrate the versatility of control theory. In hawkmoths, lateral following dynamics and luminance-dependent delays were characterized via transfer-function and frequency-domain analyses [28].

Here, we proposed and validated several candidate PID-based model structures with different sensory input combinations. A modular P/PD model showed the best performance, being inherently faster and more responsive to rapidly changing inputs [29]. Our model fitting indicates that bumblebees rely on both visual and inertial feedback when landing on moving targets, and their kinematics are effectively captured by simple modular sensory–motor control models. Moreover, the observed flight dynamics align with the helicopter model for aerodynamic force generation in insect flight [30]. These findings advance our understanding of insect landing control and inform bio-inspired UAV design.

2. Material and methods

We investigated how bumblebees land on laterally oscillating targets using behavioural experiments and control-theoretic modelling. High-speed stereoscopic videography recorded three-dimensional trajectories of *B. terrestris* landing on a sinusoidally moving flower-mimic. Deep-learning tracking extracted kinematics used to fit and validate sensory-feedback models.

2.1. Experimental work

2.1.1. Experimental animals

A *B. terrestris* hive was used for all experiments and connected to a flight arena maintained at 21 ± 2°C. The arena was illuminated with broad-spectrum LED light from 09.00 to 17.15 to enable free foraging, with light intensity gradually reduced at dusk to encourage return to the hive. The colony was fed daily with 20 g of pollen inside the hive and sugar water in the arena to promote regular foraging flights.

2.1.2. Experimental set-up

The experimental set-up comprised a *B. terrestris* hive, an octagonal flight arena ($50 \times 50 \times 48$ cm^3), a feeding platform, a hive entrance–exit system with a movable flower-mimic and a stereoscopic high-speed videography system (figure 1*a–d*). The arena is connected to the hive at one end, with a sugar-water feeder at the centre.

Downloaded from royalsocietypublishing.org/rsif/article-pdf/doi/10.1098/rsif.2025.1198/6167060/rsif.2025.1198.pdf
by guest
on 30 September 2026

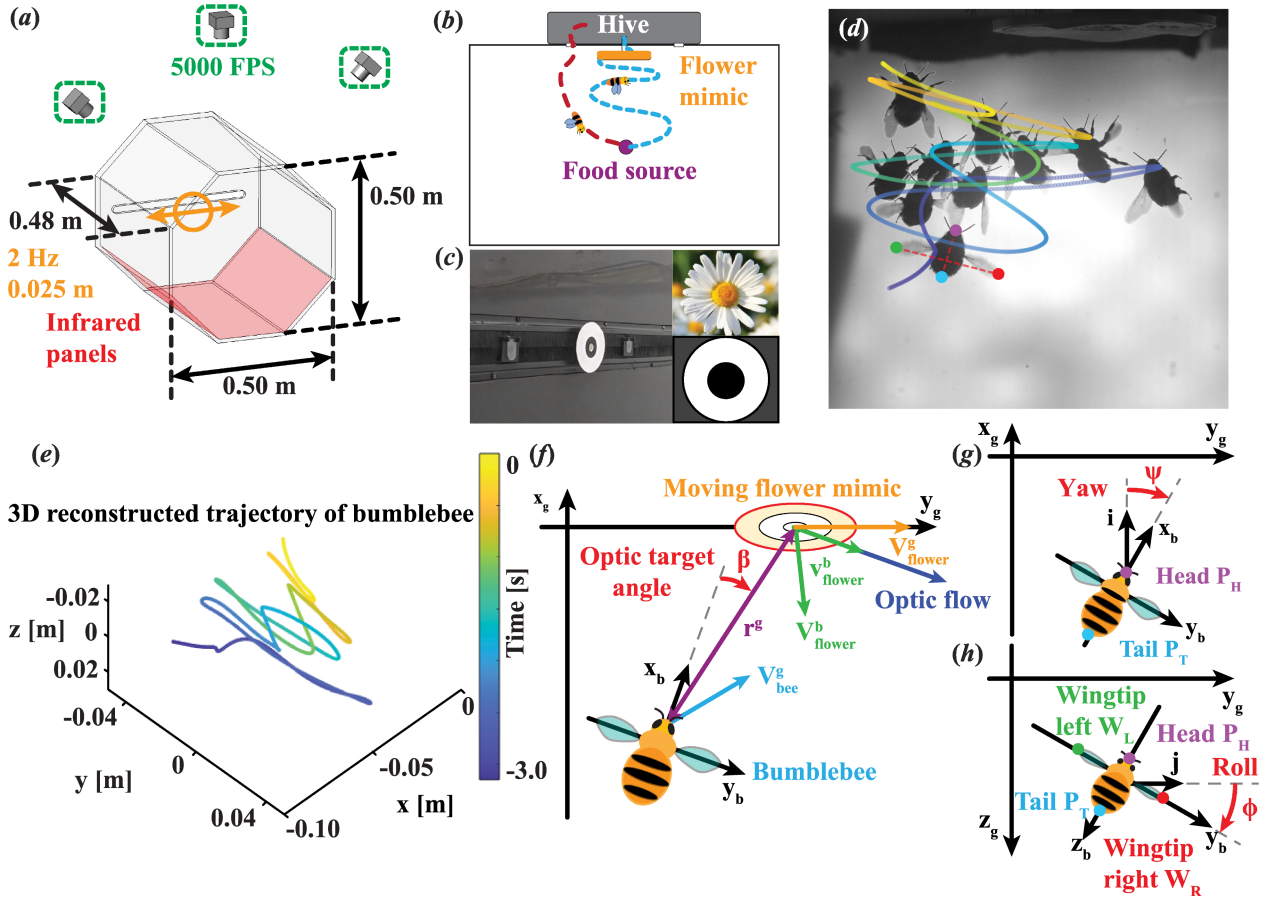


Figure 1. Experimental set-up, landing sequence and sensory–motor parameters. (*a*) Three-dimensional schematic of the octagonal flight arena (50 × 50 × 48 cm^3). The flower-mimic (orange) oscillated at 2 Hz with 0.025 m amplitude. Three high-speed cameras (5000 fps, green) and infrared LED panels (red) enabled stereoscopic imaging. (*b*) Top view of inbound foraging trajectories entering via one-way hatches (red) and return trajectories through the moving flower-mimic (blue). (*c*) The flower-mimic (figure adapted from [1]). (*d*) Example landing sequence (top view), colour-coded by time (scale in *e*). DeepLabCut tracked the flower (orange) and bee markers (head, tail and wingtips) [31]. (*e*) Reconstructed three-dimensional trajectory; $t = 0$ at touchdown. (*f*) Reference frames and visual signals: ground-fixed (x_g–y_g) aligned with flower motion; body-fixed (x_b–y_b) from tail to head and wingtip to wingtip. Optic flow OF = relative flower speed v^g_{flower}/distance $|r^g|$; optic taget angle OTA β = azimuthal angle between x_b and r^g. Uppercase V denotes a velocity vector, whereas lowercase v denotes a component along the lateral y-axis. Superscripts indicate the reference frame (g: ground-fixed and b: body-fixed). (*g*) Yaw angle ψ (clockwise positive). (*h*) Roll angle ϕ (clockwise positive).

Bees exited through a static one-way entrance and returned via a moving flower-mimic mounted on a linear stage. The circular platform, patterned with a concentric ring pattern resembling a flower (figure 1*c*), oscillated laterally at 2 Hz and 2.5 cm amplitude, driven by a stepper motor controlled via Arduino.

Landing manoeuvres were recorded using three synchronized Photron Fastcam X2 cameras (1024 × 1024 px, 5000 fps) (figure 1*a*). Cameras were positioned above the arena, facing infrared backlight panels below. Three infrared LED panels provided backlit illumination, producing high-contrast silhouettes within a 12 cm^3 recording volume (figure 1*d*; supplementary material, videos S1–S4).

2.1.3. Experimental procedure

Bumblebees were trained to consistently land on the flower-mimic before data collection. During training, bees entered the set-up, foraged and landed on the stationary flower-mimic to access the hive entrance at its centre, while the food source was gradually moved towards the arena centre. Throughout training, the flower-mimic remained static, allowing bees to associate it with the hive entrance without prior exposure to motion. This ensured that subsequent experiments better reflected natural conditions, in which flowers move irregularly owing to disturbances. Although the behavioural goal was hive re-entry rather than nectar collection, the manoeuvre still required a visually guided landing onto a defined target surface.

During experiments, bumblebees entered the flight arena through a static one-way entrance adjacent to the flower-mimic, landed on it and crawled towards its centre to exit back to the hive. Landing flights onto the moving flower-mimic were recorded over 9 days while the flower oscillated sinusoidally at 2 Hz with a mid-to-peak amplitude of 2.5 cm. Recording was manually stopped after each successful landing, and all successful landing sequences were saved, where the segment from first appearance to touchdown was exported as a TIFF sequence.

Downloaded from royalsocietypublishing.org/rsif/article-pdf/doi/10.1098/rsif.2025.1198/6167060/rsif.2025.1198.pdf
by guest
on 30 September 2026

2.2. Kinematic tracking and sensory input signals

2.2.1. Tracking the trajectories of the landing bumblebees and the flower-mimic

Three-dimensional trajectories of the bumblebees and flower-mimics were extracted from stereoscopic recordings using a deep-learning tracking approach. Videos were down-sampled from 5000 to 500 Hz and processed with DeepLabCut [31], which achieves approximately 2.7 pixel (human-level) accuracy with approximately 500 frames. In each sequence, head and tail positions were tracked to reconstruct body motion (supplementary material, video S5); for the 10 longest flights, both wingtips were additionally tracked to estimate body roll kinematics (supplementary material, video S6). The leftmost and rightmost points of the flower-mimic were tracked in all sequences to quantify its oscillatory motion (supplementary material, video S5).

2.2.2. Calibration and three-dimensional reconstruction

Prior to three-dimensional reconstruction, the videography dataset was calibrated using **EasyWand5** [32]. A T-shaped wand with two pinheads 6 cm apart served as the calibration object and was moved throughout the recording volume. Pinhead positions were tracked across calibration videos to compute the direct-linear-transformation parameters for each camera. Using these parameters and DeepLabCut tracking results, three-dimensional trajectories of the bumblebee and flower-mimic were reconstructed [33]. An example head trajectory is shown in figure 1*e*.

2.2.3. Coordinate system definition and kinematic derivation

Trajectories of the flower-mimic and bumblebee were expressed in two coordinate systems. The ground-fixed frame (x_g–y_g) was centred at the flower's mid-position, with y_g aligned with its motion and x_g pointing outward from the arena (figure 1*f*). The body-fixed frame (x_b–y_b) was centred on the bee, with x_b oriented tail-to-head and y_b from left to right wingtip (figure 1*f*–*h*). Time was defined per flight sequence with $t = 0$ s at touchdown. Hereafter, kinematics refers to body kinematics (position and orientation) only, not wing kinematics.

Kinematics were analysed in the ground-fixed frame. Flower position was defined by the midpoint between the left and right markers, and bee kinematics were derived from head, tail and wingtip positions. Velocities $V(t)$ and accelerations $A(t)$ were computed from position vectors $X(t)$ using a second-order central difference scheme. Uppercase V denotes a velocity vector, whereas lowercase v denotes a component along a specified axis (here, the lateral y-axis). Superscripts indicate the reference frame (g: ground-fixed and b: body-fixed). Accordingly, V^g_{bee} and V^g_{flower} denote bee and flower velocities in the ground-fixed frame, respectively, while V^b_{flower} and v^b_{flower} represent the flower velocity and its lateral component in the body-fixed frame, respectively.

To reduce noise amplification from differentiation, velocity and acceleration data were low-pass filtered with an eighth-order Butterworth filter (**MATLAB** *butter*) at a 10 Hz cut-off frequency. To avoid phase distortions, filtering was performed using the zero-phase *filtfilt* procedure, which applies the filter forwards and backwards in time.

2.2.4. Body attitude angles

To quantify the bumblebee's body orientation during landing, we estimated its attitude angles relative to the ground-fixed reference frame. Using the head and tail positions, we derived the yaw angle ψ as the angle between the head–tail vector and the x_g-axis.

The 10 longest sequences, defined by the number of frames prior to touchdown, were used for roll reconstruction. For these sequences, roll angle ϕ was estimated from the left and right wingtip positions, as the angle between the wingtip vector and the y_g-axis.

2.2.5. Sensory input signals

To examine how bumblebees employ sensory–motor control to aim at and align with the flower, we estimated two visual inputs: OTA (β) and OF, and one inertial input, yaw rate ($\dot{\psi}$), from the reconstructed kinematics of the bumblebee and flower-mimic.

OF, defined as the relative sideways velocity divided by distance [9], was estimated by the lateral component of the flower-mimic relative velocity in the body-fixed frame, v^b_{flower} with separation distance $|r^g|$ as (see supplementary material for details)

$$OF = v^b_{flower}/|r^g|, \tag{2.1}$$

which corresponds to an angular velocity (rad s^{-1}) describing the relative lateral motion of the flower-mimic on the retina. For visualization, this quantity was converted to degrees per second in the following sections.

The second visual input, the OTA (β), was defined as the viewing angle of the flower-mimic in the bumblebee's visual azimuth plane, with $\beta = 0°$ when the target was centred (clockwise positive, figure 1*f*).

The inertial input signal used in this work is the yaw rate ($\dot{\psi}$). We estimated that simply by differentiating the derived time histories of yaw angle with a second-order numerical central difference scheme.

Downloaded from royalsocietypublishing.org/rsif/article-pdf/doi/10.1098/rsif.2025.1198/6167060/rsif.2025.1198.pdf
by guest
on 30 September 2026

2.3. Modelling the sensory–motor control

Sideways-movement and gaze-control models were implemented in **MATLAB Simulink**, and parameters were estimated using the **parameter estimation** toolbox. Model parameters were fitted for each sequence, and the resulting simulations were exported for further analysis. To identify the simplest accurate model, we applied iterative pruning. Starting from a full model containing all candidate sensory pathways (OF proportional and derivative terms, OTA and yaw rate), individual pathways were sequentially removed and re-estimated. Performance was evaluated via correlation and residual analyses, and non-contributing pathways were discarded to obtain compact, biologically plausible models. Importantly, the estimated delay τ reflects an effective closed-loop model-fitting delay that captures the aggregate input–output latency of the system, including sensory, motor and biomechanical dynamics, and should not be interpreted as a direct neural delay.

2.4. Sensory–motor control model simulations

To validate the sideways-movement and gaze-control models, we conducted numerical simulations under simplified conditions to test whether the fitted models reproduced observed dynamics and exhibited static stability. Each model was implemented in **MATLAB Simulink** using estimated parameters and simulated with both sequence-specific and median values to assess generality. Input signals (OF and yaw rate) were derived from experimental data or analytically generated (e.g. constant approach speed and sinusoidal flower motion) to isolate sensory contributions.

We then examined each model's initial response when the bumblebee entered the field of view without initial rotation. These analyses tested whether the proposed feedback structures generated corrective yaw accelerations in the appropriate direction, indicating static stability of gaze control.

2.5. Statistical analysis

Data were analysed using (paired) *t*-tests, and results are reported as *median* [*95% confidence interval*]. Statistical significance was defined as $p < 0.05$.

3. Results

We tracked the three-dimensional flight trajectories of 48 bumblebees landing on the moving flower-mimic (figure 1*d,e*). From these recordings, we extracted sideways flight kinematics and body yaw rotations (figures 2 and 3). For the 10 longest landing sequences, body roll kinematics were also analysed. Control-theoretic modelling was then used to investigate how bumblebees regulate sideways movement and gaze during landing on moving flowers. Results are presented in three parts: (i) landing kinematics, (ii) sensory–motor control modelling, and (iii) simulations based on the derived models.

3.1. Experimental results for bumblebees landing on rapidly moving flowers

Throughout the experimental results section, we show detailed data of a single stereotypic landing as an example (figure 1*d,e*; supplementary material, videos S1–S6), and summarize statistics of all landing manoeuvres.

3.1.1. Sideways-movement kinematics for tracking rapidly moving flowers

Time series of the landing bumblebee and flower-mimic sideways motion were decomposed into position, velocity and acceleration components (representative example in figure 2*a–c*). The flower-mimic oscillated sinusoidally at 2 Hz with a 2.5 cm amplitude, peak velocity of 0.31 m s^{-1} and peak acceleration of 3.95 m s^{-2}. Landing bumblebees closely matched these kinematics, exhibiting comparable amplitudes, velocities and accelerations of 2.66 cm, 0.32 m s^{-1} and 4.00 m s^{-2}, respectively, but their sideways oscillations consistently lagged the flower motion (figure 2*a–c*). When flower kinematics were shifted by an approximately estimated 100 ms delay, the overlap between flower and bee trajectories became nearly perfect (figure 2*e–g*). This manually applied shift serves only as a qualitative illustration of temporal alignment and is not a quantitative estimate of sensory–motor delay. The consistent overlap throughout the landing manoeuvre argues against predictive flower tracking and instead suggests that bumblebees align their sideways kinematics with perceived target motion, resulting in an inherent sensory–motor delay between flower and animal.

Repeating this analysis across all landings revealed similar sideways kinematics. Velocity oscillation amplitudes were significantly greater than those of the flower-mimic, whereas position and acceleration amplitudes were not (figure2*h–j*). Bumblebee velocity amplitudes were 13% larger than those of the flower (v^{g}_{bee} = 0.36 [0.32–0.40] m s^{-1}, $p = 0.01$). By contrast, positional and acceleration amplitudes were comparable (y^{g}_{bee} = 2.80 [2.57–3.10] cm, $p = 0.26$; $a^{g}_{y,bee}$ = 3.99 [3.54–4.55] m s^{-2}, $p = 0.96$). These results indicate that sideways position and acceleration closely matched flower motion, whereas velocity exhibited slight overshoots.

Downloaded from royalsocietypublishing.org/rsif/article-pdf/doi/10.1098/rsif.2025.1198/6167060/rsif.2025.1198.pdf
by guest
on 30 September 2026

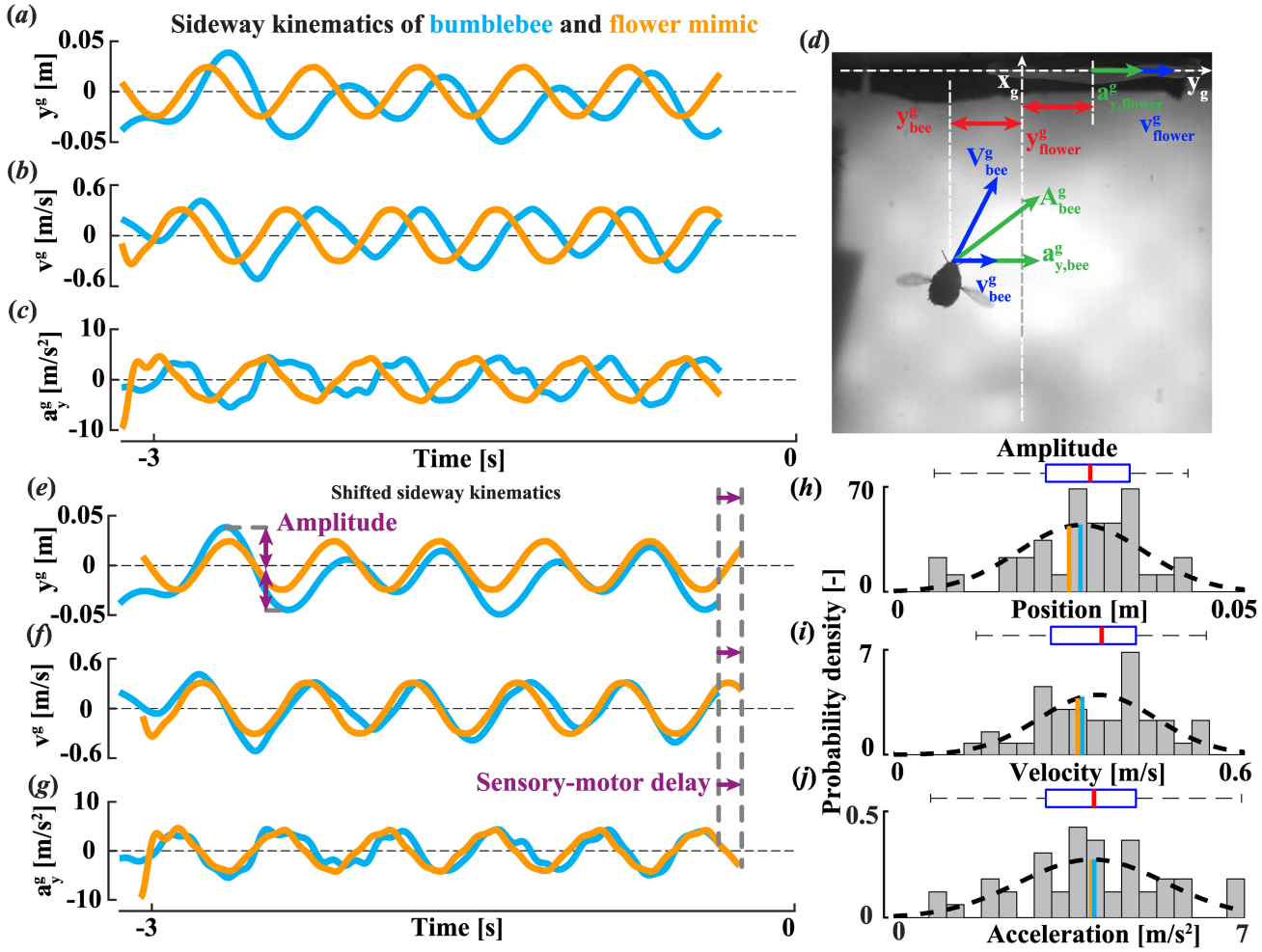


Figure 2. Sideways flight kinematics of bumblebees landing on the moving flower-mimic. (*a–c*) Sideways position (*a*), velocity (*b*) and acceleration (*c*) of the bumblebee (blue) and flower-mimic (orange), during the example landing. (*d*) Kinematic variables used for analysis. (*e–g*) Flower data shifted by 100 ms align closely with bee kinematics. (*h–j*) Amplitude distributions of (*h*) position, (*i*) speed and (*j*) acceleration for the flower (orange), example bumblebee (blue), and all 48 sequences (grey). Bees show significantly larger speed amplitudes than the flower.

3.1.2. Body attitude kinematics for tracking rapidly moving flowers

Accurate flower tracking requires control of both position and orientation. We therefore quantified body yaw and roll kinematics during landings (figure 3). In the example case, yaw and roll angles oscillated periodically with sideways motion (figure 3*a*,*d*), reaching amplitudes of 19° and 27°, respectively. These rapid oscillations were associated with large transient rotational rates and accelerations about both axes (figure 3*a–f*).

Across all landings, yaw angle oscillations were consistent with the example case (figure 3*g–i*), with an amplitude of $A_\psi = 26°$ [24–28°]. These rotations resulted from large yaw rates and accelerations ($\dot{\psi} = 300°$ [266–382°] s^{-1}; $\ddot{\psi} = 8.1°$ [7.4–8.9°] $\times 10^3$ s^{-2}).

Roll kinematics, analysed for the 10 longest landing sequences, showed similar oscillations (figure 3*j–l*). The roll amplitude was $A_\phi = 31°$ [27–33°], driven by rapid roll rates and accelerations ($\dot{\phi} = 575°$ [465–743°] s^{-1}; $\ddot{\phi} = 14.3°$ [11.8–16.2°] $\times 10^3$ s^{-2}). These wide ranges of body attitude angles and their periodic oscillations indicate that bumblebees repeatedly adjust heading and bank angle to align with the moving flower-mimic during landing.

3.1.3. Visual input dynamics of bumblebees tracking a rapidly moving flower

To land on a moving flower, bumblebees rely on sensory–motor control to aim at and align their motion with the target [1]. We therefore analysed the temporal dynamics of visual cues generated by the moving flower-mimic during landing (figure 4). Specifically, we quantified OTA in the body frame and OF perceived during the manoeuvre (figure 1*f*) [34].

In the example landing, both OF and OTA oscillated periodically with amplitudes of $A_{OF} = 387°$ s^{-1} and $A_\beta = 18°$, respectively (figure 4*a*,*b*). These visual dynamics closely matched sideways flight kinematics. OF magnitude increased slightly as the bee approached the flower-mimic, consistent with its inverse dependence on target distance (equation (2.1)).

Downloaded from royalsocietypublishing.org/rsif/article-pdf/doi/10.1098/rsif.2025.1198/6167060/rsif.2025.1198.pdf
by guest
on 30 September 2026

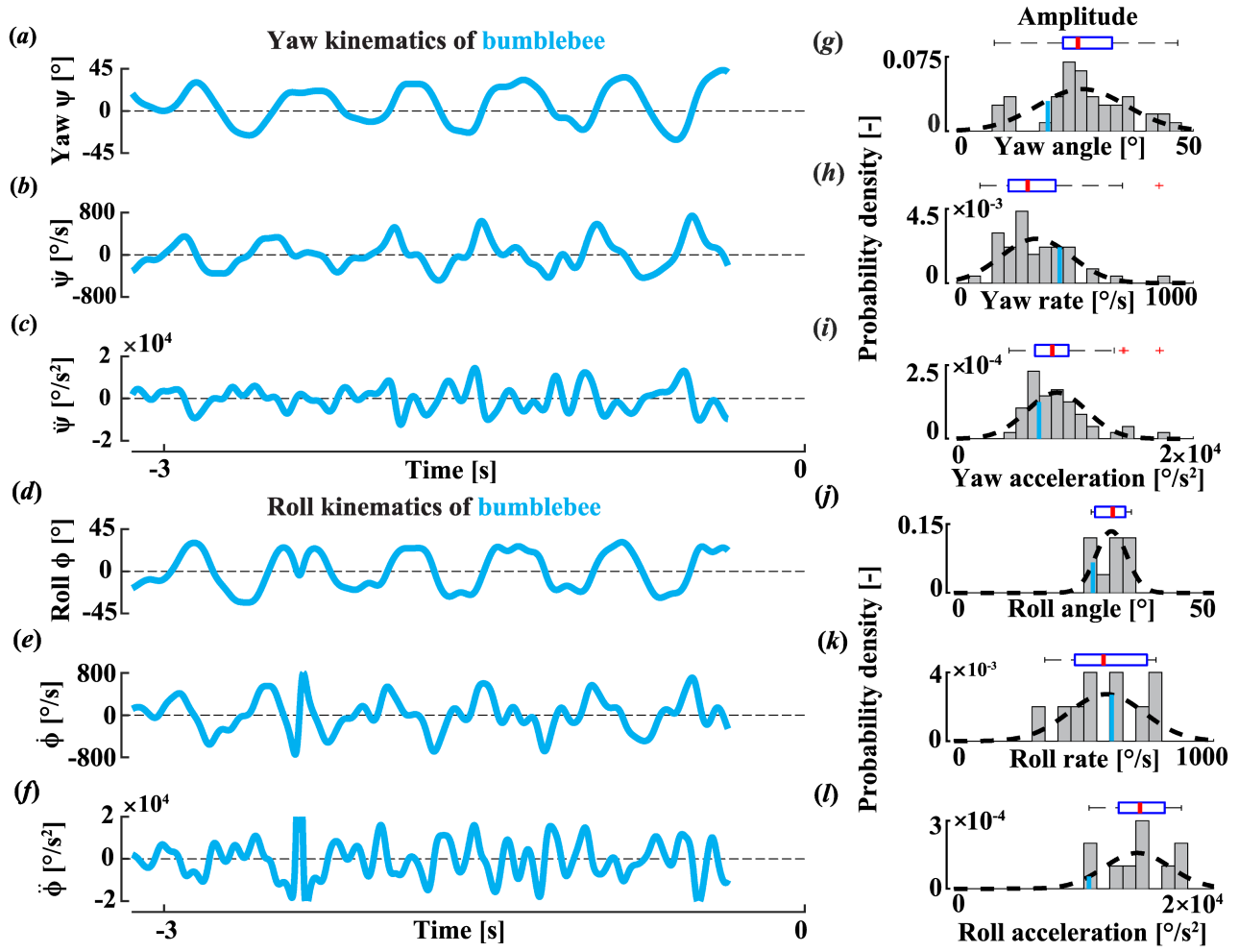


Figure 3. Yaw and roll kinematics of bumblebees landing on a moving flower-mimic. (*a–c*) Yaw angle ψ, rate $\dot{\psi}$ and acceleration $\ddot{\psi}$ during the example landing. (*d–f*) Equivalent roll angle ϕ, rate $\dot{\phi}$ and acceleration $\ddot{\phi}$. (*g–i*) Distributions of yaw angle, rate and acceleration amplitudes for 48 landings. (*j–l*) Distributions of roll angle, rate and acceleration amplitudes for the 10 longest landings. Example case in blue.

Across all landings, OF and OTA amplitudes were similar to the example case (A_{OF} = 324° [262–372°] s^{-1}; A_{β} = 21° [18–23°] (figure 4*c*,*d*)). These results indicate that bumblebees experience strong OF and large OTA deviations during landing, supporting the hypothesis that bees align their sideways kinematics with perceived flower motion rather than predicting it, with sensory–motor delay inherently producing the observed deviations.

3.2. Sensory–motor control modelling

Experimental data suggest that bumblebees may use reactive sensory–motor feedback to land on moving targets. We therefore applied classical control theory to model this system. Sideways movement and yaw-based gaze control were modelled separately. In both cases, we started with a full sensory–motor model and iteratively removed components to identify the minimal model that accurately reproduced the observed motor responses.

3.2.1. Modelling sideways-movement control in landing bumblebees

To land on a laterally moving flower, bumblebees must align their sideways motion with the target. We hypothesized that OF is used to track flower movement, complemented by angular yaw-rate feedback ($\dot{\psi}$) to counteract these rotational effects and stabilize visual perception.

To model the translational sideways-following behaviour, we first considered a full PD control model with OF and yaw rate as sensory inputs and sideways acceleration as motor output (figure 5*a*). The model contains three parameters: the proportional-gain K_p, derivative-gain K_d and sensory–motor delay τ_{pd}, which were estimated individually for all landing sequences, including the example case (figure 5*c*,*e*).

In the example case, the PD model reproduced the observed sideways acceleration closely (figure 5*c*). However, analysis of pathway outputs revealed that the amplitude of the derivative-pathway output is negligibly small compared to the

Downloaded from royalsocietypublishing.org/rsif/article-pdf/doi/10.1098/rsif.2025.1198/6167060/rsif.2025.1198.pdf
by guest
on 30 September 2026

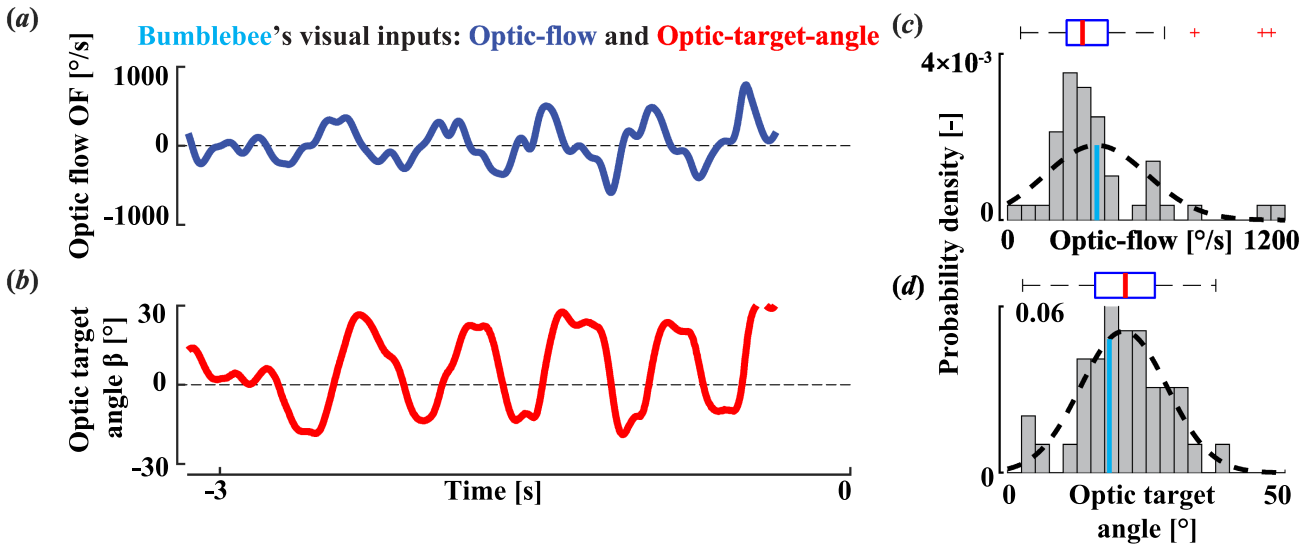


Figure 4. Visual input of the moving flower-mimic perceived by bumblebees. (*a*,*b*) Temporal dynamics of optic flow OF (*a*) and optic target angle OTA β (*b*) during the example landing, both showing periodic oscillations. (*c*,*d*) Distributions of OF (*c*) and OTA β (*d*) amplitudes for all 48 landings; example case in blue.

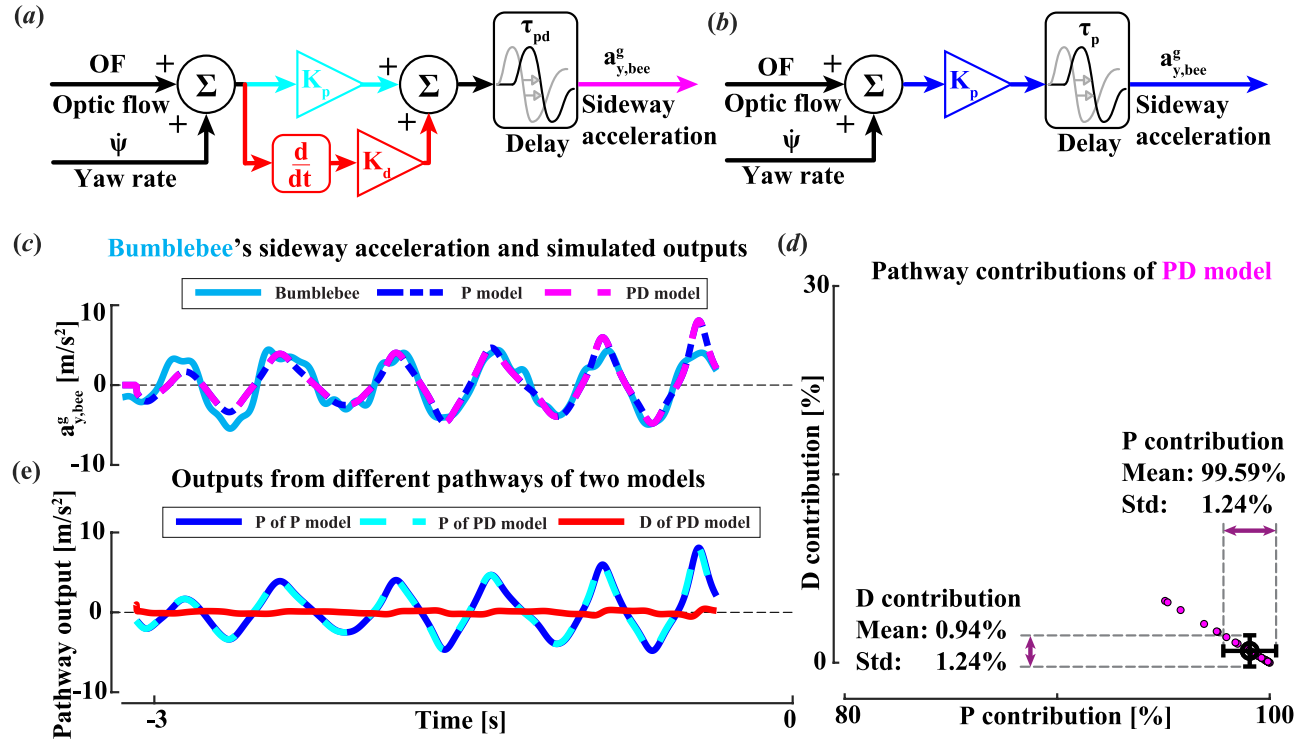


Figure 5. Modelling sideways-movement control in landing bumblebees. (*a*,*b*) Schematics of the PD model (*a*) and P model (*b*) for sideways control. In the PD model, OF and yaw-rate inputs pass through proportional and derivative pathways whose outputs are summed and delayed to produce sideways acceleration. The P model omits the derivative pathway. (*c*,*d*) Example landing: (*c*) measured sideways acceleration (light blue) compared with PD-model (magenta) and P-model (blue) outputs from the combined OF and yaw-rate inputs, both matching well. (*d*) Pathway contributions to model output, showing a negligible derivative term. (*e*) Among 48 sequences, the P pathway accounts for 99.6% of output, whereas the D pathway contributes only 0.9%.

proportional-pathway outputs (figure 5*e*). Across all 48 landings, the derivative pathway contributed only 0.9 ± 1.2% of the output, whereas the proportional pathway accounted for 99.6 ± 1.2% (figure 5*d*).

Given the minimal contribution of the derivative component, we evaluated a simplified proportional (P) model without the derivative component (figure 5*b*). For the example landing, the P model produced nearly identical acceleration and pathway outputs to those of the PD model (figure 5*c*,*e*), indicating that proportional feedback alone accurately captures sideways control. The P model was therefore used for subsequent analyses (figure 6).

Parameter estimation of the P model yielded narrow distributions for both K_p and τ_p (figure 6*c*), which further indicates the stable convergence of parameter estimation and model validity. Median parameter values (K_p = 0.40 and τ_p = 54.00 ms

Downloaded from royalsocietypublishing.org/rsif/article-pdf/doi/10.1098/rsif.2025.1198/6167060/rsif.2025.1198.pdf
by guest
on 30 September 2026

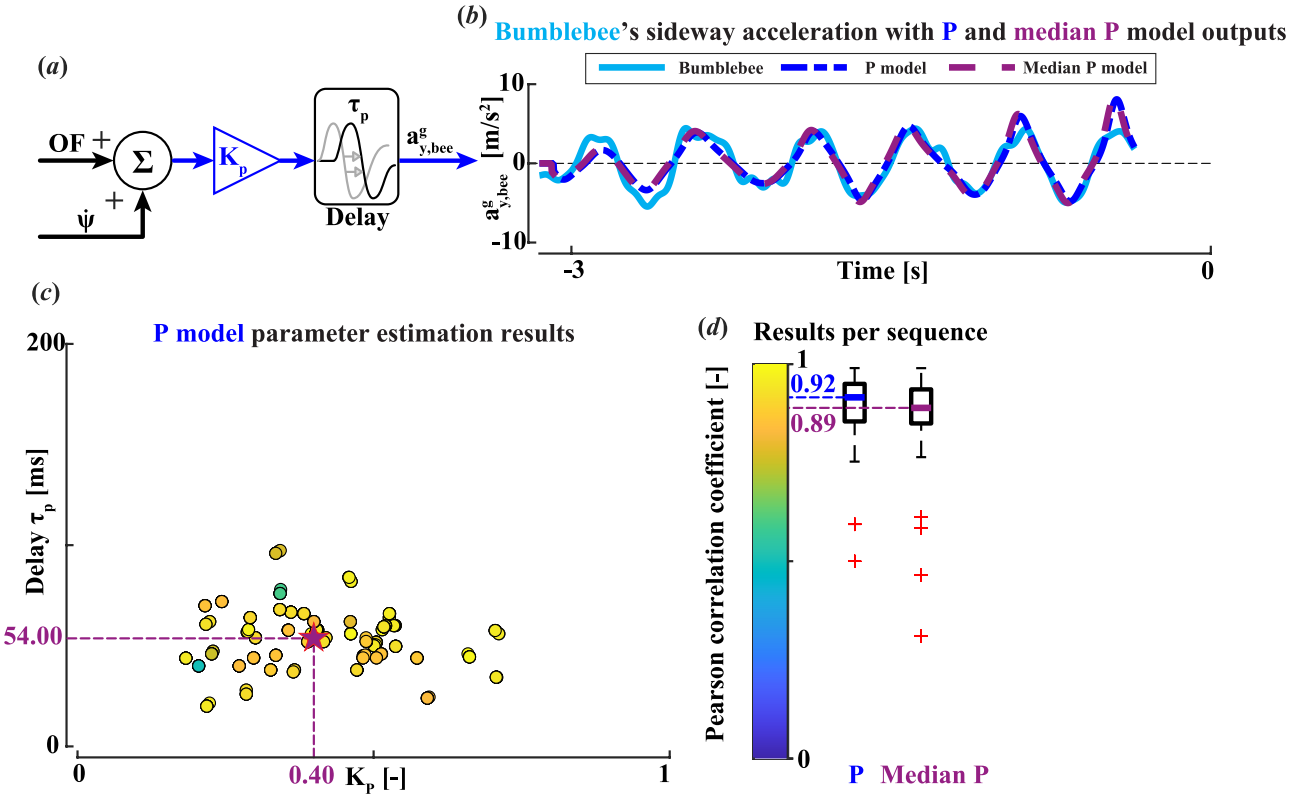


Figure 6. Sideways movements of bumblebees landing on a moving flower captured by a proportional controller. (*a*) Diagram of the P model for sideways movement. (*b*) Example sequence: bee's sideways acceleration (light blue) compared with outputs of sequence-specific P model (dark blue) and median P model (purple). (*c*) Distributions of proportional-gain K_p and delay τ_p for all 48 sequences, colour-coded by Pearson correlation *r*; median case marked with a star ($K_p = 0.40$ and $\tau_p = 54$ ms). (*d*) Performance comparison between sequence-specific and median P models: the median model has slightly lower Pearson correlation (paired *t*-test; $p < 0.001$).

(figure 6*c*)), obtained independently for each parameter from their respective distributions across sequences, were used to construct a so-called median P model.

For the example sequence, the median P model reproduced the observed acceleration closely, matching the sequence-specific model (figure 6*b*). To compare model performance, we calculated Pearson correlation coefficients (*r*) between simulated outputs and measured sideways accelerations (figure 6*d*). Among all landings, the median P model yielded slightly lower correlations than sequence-specific models ($r = 0.89$ [0.88–0.90] versus $r = 0.92$ [0.91–0.92]; $p < 0.001$). These results indicate that the median P model performs comparably to sequence-specific models and effectively captures bumblebee sideways-following control.

3.2.2. Roll angle and lateral acceleration production

Aerodynamic force control in insect flight is often described by the helicopter model [30], which posits that insects generate horizontal acceleration by tilting their body to redirect the aerodynamic force vector, analogous to helicopter thrust vectoring. This model has been validated for dipterans [35] and hawkmoths [36]. Following this framework, we analysed roll-angle time histories from 10 longest landing sequences to examine how bumblebees generate lateral acceleration.

According to the model (figure 7*a*,*b*), lateral acceleration $a^g_{sideway}$ arises from roll angle (ϕ) as

$$a^g_{sideway} = g \tan(\phi), \tag{3.1}$$

where $g = 9.81$ m s^{-2}. For the example landing, model-predicted accelerations closely matched the measured values (figure 7*d*). Across all 10 sequences, predicted and measured acceleration amplitudes agreed well (figure 7*c*), yielding high Pearson correlations ($r = 0.91$ [0.89–0.94] (figure 7*e*)). These results indicate that bumblebees generate lateral acceleration by modulating roll angle, consistent with the helicopter model of insect aerodynamic force production.

3.2.3. Modelling yaw kinematics for gaze control in landing bumblebees

In addition to aligning sideways movements, bumblebees must aim towards and maintain gaze on the flower during landing by actively adjusting yaw angle ψ. We hypothesized that yaw dynamics are regulated using OTA (β), OF and yaw-rate ($\dot{\psi}$) feedback.

Downloaded from royalsocietypublishing.org/rsif/article-pdf/doi/10.1098/rsif.2025.1198/6167060/rsif.2025.1198.pdf
by guest
on 30 September 2026

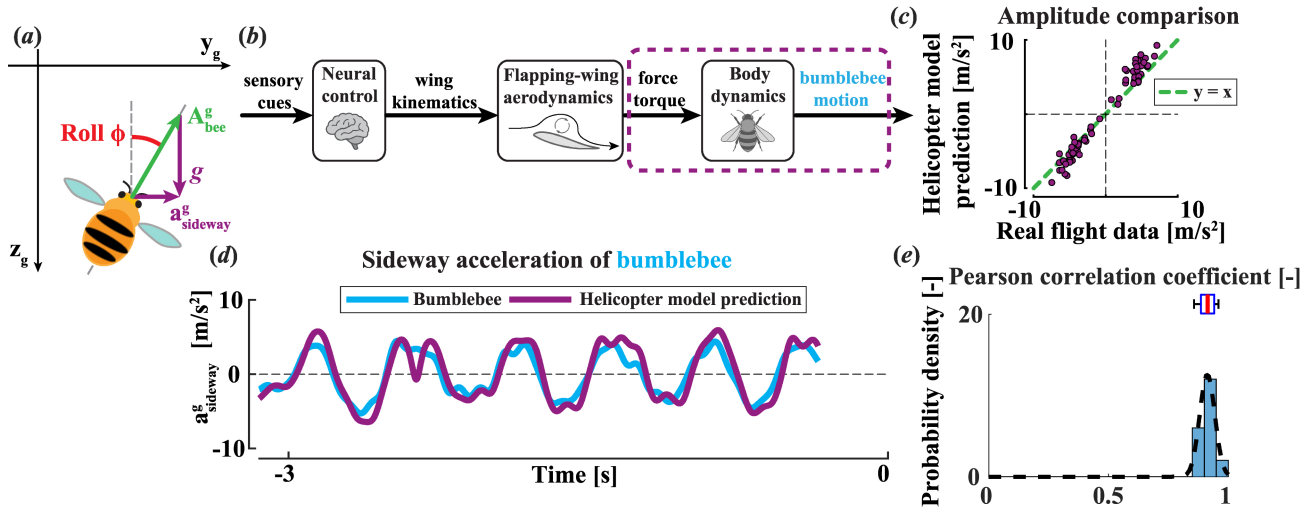


Figure 7. Bumblebees control sideways movements using body roll kinematics. (*a*) Helicopter model illustrates how insects generate lateral acceleration by rolling their body to redirect aerodynamic force; predicted acceleration is $a^{g}_{sideway} = g\tan(\phi)$. (*b*) Neural control processes sensory cues to adjust wing kinematics, producing torques, redirecting the aerodynamic force vector. (*c*) Example landing: measured lateral acceleration (blue) and model prediction (purple) show close agreement. (*d*) Comparison of amplitudes from model predictions and measurements for the 10 longest sequences; points cluster near the identity line. (*e*) Pearson correlation coefficients *r* between model and measured accelerations are close to 1 across sequences.

To test this, we developed an optic-gaze yaw model (gaze control) incorporating visual and inertial inputs, with yaw acceleration ($\ddot{\psi}$) as output. We first considered a full model including OTA (β), OF (processed via a PD controller) and yaw-rate ($\dot{\psi}$) inputs (figure 8*a*). Fitting this model to flight data required estimating five parameters: OF proportional (K_p) and derivative (K_d) gains, OTA gain (K_β), yaw-rate gain (($K_{\dot{\psi}}$) and delay ($\tau_{\dot{\psi}}$). Parameter estimation showed strong model performance ($r = 0.86$ [0.85–0.86]; supplementary material, table S6).

Pathway contribution analysis revealed that the OTA pathway contributed negligibly (0.4‰[0.2–0.5‰] (figure 8*c*,*d*)) and was therefore removed. The resulting reduced model retained OF and yaw-rate inputs (figure 8*b*). This negligible positional contribution suggests that gaze control is dominated by motion-dependent cues rather than static retinal position. Similar motion-based mechanisms have been reported in *Drosophila*, where positional centring emerges from optomotor feedback and motion pathways [10–12].

Three additional candidate models were further tested by sequentially removing remaining pathways (figure 8*b*). In all cases, model performance declined substantially (supplementary material, table S6), indicating that the final gaze-control model requires proportional OF, OF derivative and yaw-rate pathways.

The simulated output closely matched the observed yaw acceleration (figure 8*c*). Unlike the sideways model, all pathways contributed substantially to the output (figure 8*e*), with yaw-rate feedback dominating (48.0% [39.8–55.2%]), followed by OF derivative (36.2% [28.1–43.9%]) and OF proportional pathways (9.7% [6.3–14.7%]).

Parameter estimation results showed limited variability, with values tightly clustered around their medians (figure 9*c*). Using the median parameter values ($K_{\dot{\psi}} = -13.59$, $K_d = 0.58$, $K_p = 6.48$ and $\tau_{\dot{\psi}} = 52.02$ ms) obtained independently for each parameter from their respective distributions across sequences, we constructed the median gaze-control model and applied it to all sequences.

For the example landing, the median model reproduced both the experimental kinematics and the sequence-specific model output (figure 9*b*). Across all sequences, correlations between simulated and observed yaw accelerations were slightly lower but comparable to those of sequence-specific models ($r = 0.82$ [0.81–0.82] versus $r = 0.86$ [0.85–0.87]; $p < 0.0001$ (figure 9*d*)). These results indicate that the median model effectively captures bumblebee yaw-control dynamics.

3.3. Simulating landing kinematics based on sensory–motor control models

We tested the fidelity and stability of the developed sensory–motor control models with simulations, both for sideways-movement control and yaw-based gaze control.

3.3.1. Simulating sideways movement based on the sensory–motor control model

In this work, sideways movements of bumblebees landing on a moving flower-mimic are well captured by a P model with OF and yaw-rate inputs (§3.2.1). Based on scalar calculations (figure 10*a*), the OF generated by relative sideways movements between the bee and flower-mimic ($OF_{sideway}$) can be approximated from OF perceived in the body-fixed frame and yaw rate as

$$OF_{sideway} \approx OF + \dot{\psi}. \tag{3.2}$$

Downloaded from royalsocietypublishing.org/rsif/article-pdf/doi/10.1098/rsif.2025.1198/6167060/rsif.2025.1198.pdf
by guest
on 30 September 2026

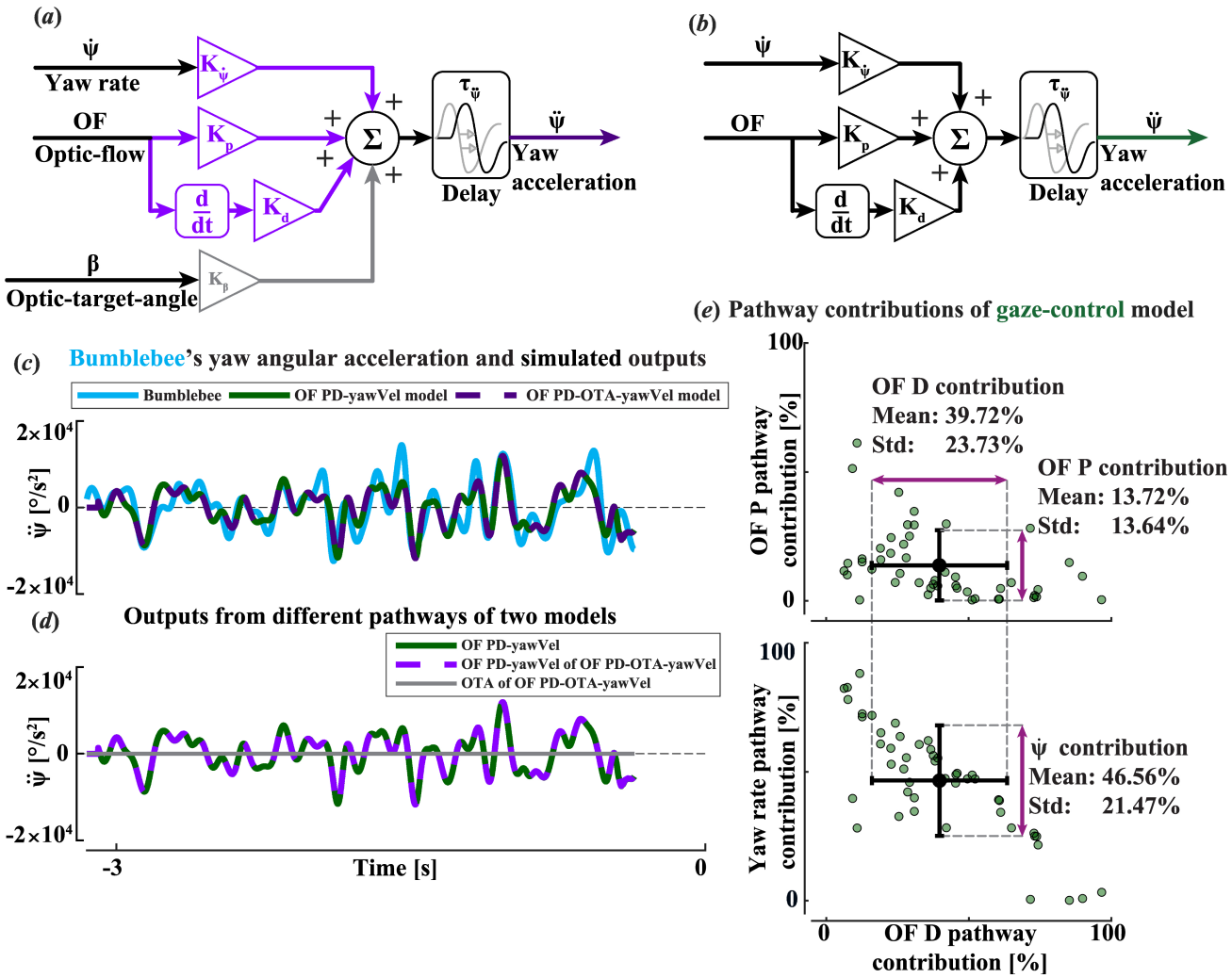


Figure 8. Modelling yaw-based gaze control of landing bumblebees. (*a*,*b*) Diagrams of two candidate models. The full model (*a*) includes OF, OTA and yaw rate; OF passes through a PD controller, and all inputs are summed and delayed to produce yaw acceleration. The reduced model (*b*) removes the OTA input. (*c*) Example landing: measured yaw acceleration (blue) compared with outputs of the full model (purple) and reduced model (green), both reproducing the oscillatory pattern with slightly lower amplitudes. (*d*,*e*) Contributions to model output. (*d*) The OTA pathway of the full model (grey) contributes negligibly, whereas other components are similar between models. (*e*) Across 48 sequences in the reduced model, yaw rate contributes 47%, OF derivative 40% and proportional OF 14%.

To test this, we simulated flower tracking using the sideways P model and compared the summed OF and yaw-rate ($\dot{\psi}$) signals with measured $OF_{sideway}$. In the example case, the combined signal closely matched the measured $OF_{sideway}$ (figure 10*b*). Across all sequences, the relationship (equation (3.2)) was consistently supported, with Pearson correlation coefficients not significantly different from unity ($r = 0.99$ [0.99–1.0] (figure 10*c*)). These results suggest that bumblebees likely integrate OF and yaw-rate feedback to estimate their sideways motion relative to the flower-mimic in the inertial frame.

3.3.2. Simulating gaze-control dynamics based on the yaw-control model

To evaluate the static stability of the gaze-control model, we performed simulations using the OF PD yaw-control model. These examined the initial yaw-acceleration response when bumblebees entered the camera's field of view without body rotation ($\dot{\psi} = 0$ (figure 11*a*)). Substituting the static-stability condition (negative initial slope where $\ddot{\psi} = 0$ at $y^g_{bee} = 0$) into the controller output yields the proportional-to-derivative gain ratio (see supplementary material for details):

$$k = \frac{K_p}{K_d} = \frac{|V^g_{approach}|}{x^g_{bee}} - \frac{a^g_{y,flower}}{|v^g_{flower}|}. \tag{3.3}$$

Perfect static stability, therefore, requires the PD gain ratio to match the right-hand side of equation (3.3). In simulations, approach speed was fixed to the mean value ($|V^g_{approach}| = 0.02\ m\ s^{-1}$), and flower velocity and acceleration were set to their mean values over half a period ($|v^g_{flower}| = 0.16\ m\ s^{-1}$ and $a^g_{y,flower} = -1.97\ m\ s^{-2}$). Here, the negative acceleration indicates acceleration in the negative y_g direction. Simulations were initialized at three approach distances ($x^g_{bee} = [-0.12, -0.10, -0.08]$ m) and two lateral

Downloaded from royalsocietypublishing.org/rsif/article-pdf/doi/10.1098/rsif.2025.1198/6167060/rsif.2025.1198.pdf
by guest
on 30 September 2026

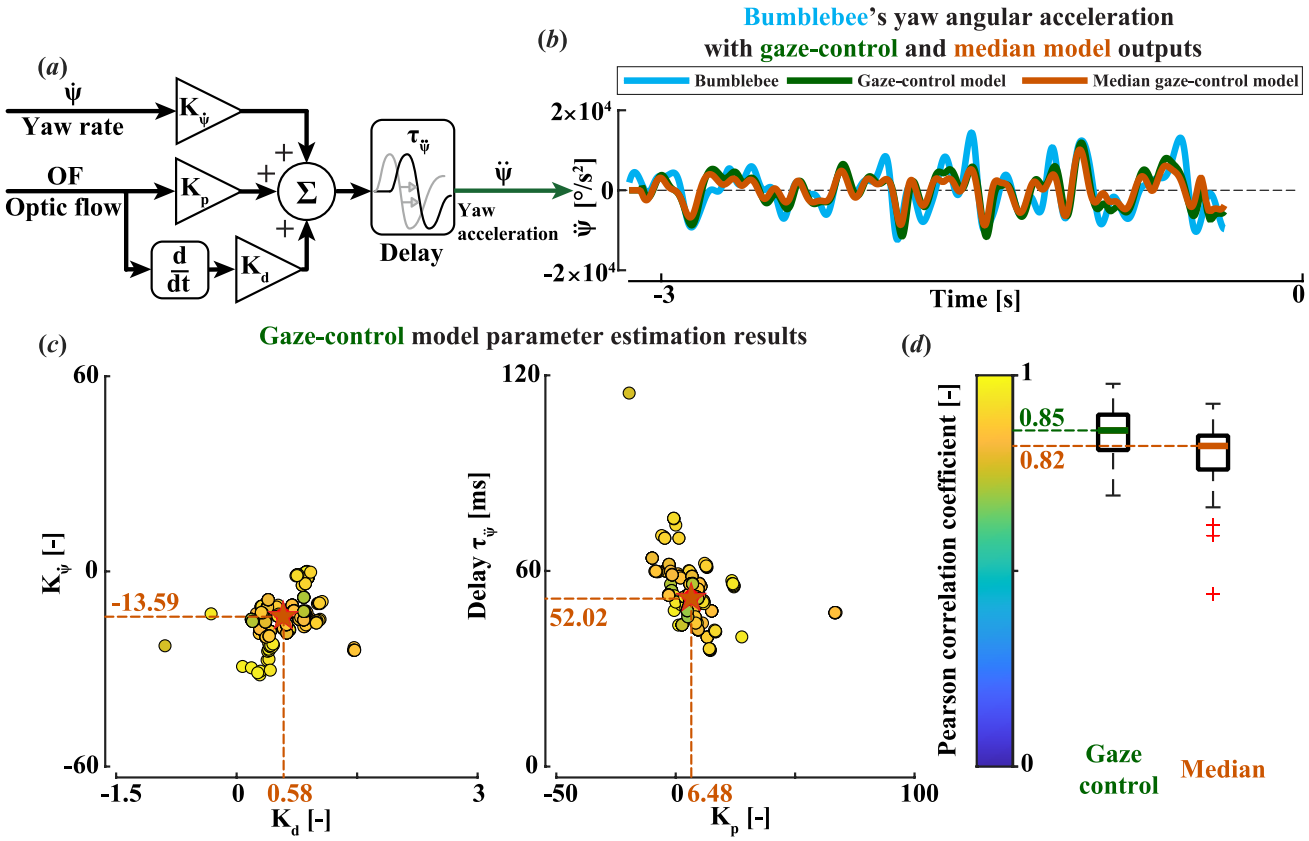


Figure 9. Yaw-based gaze control of bumblebees landing on a moving flower captured by a PD model. (*a*) Diagram of the reduced sensory–motor model for gaze control. (*b*) Example landing: yaw acceleration (blue) compared with outputs of the sequence-specific model (green) and median model (orange). Both replicate the oscillatory pattern, though the median model shows slightly lower amplitudes. (*c*) Distributions of OF proportional-gain (K_p), derivative-gain (K_p), yaw-rate gain ($K_{\dot\psi}$) and delay ($\tau_{\ddot\psi}$) across 48 sequences, colour-coded with Pearson's correlation coefficient; star denotes the median. (*d*) Model performance comparison shows slightly higher accuracy of sequence-specific models than that of the median model.

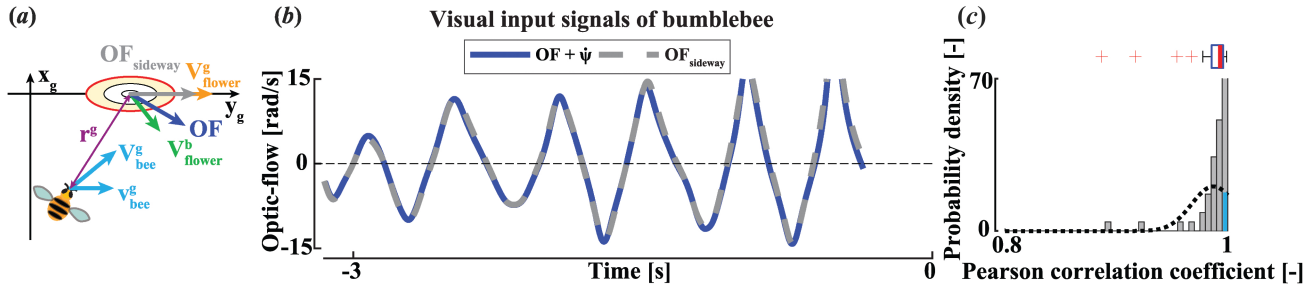


Figure 10. Landing bumblebees use both visual and mechanosensory feedbacks to track a moving flower. (*a*) Bee and landing platform illustrate OF and sideways OF ($OF_{sideway}$). (*b*) Example case: time history of OF + $\dot\psi$ compared with $OF_{sideway}$, showing near-perfect overlap. (*c*) Distributions of Pearson correlation coefficients *r* between the combined signal (OF + $\dot\psi$) and $OF_{sideway}$ across 48 sequences; the example case is highlighted in blue.

offsets (y^g_{bee} = [−0.05, 0.05] m). Substituting these values into equation (3.3) yielded *k* = [12.30–12.40]. With the median proportional-gain (K_p = 6.48), this corresponds to K_d = [0.52–0.53], which lies within the 95% interval K_d = [0.51–0.62]. We therefore adopted K_p = 6.48 and K_d = 0.53.

Using these parameters, simulations showed that when bees entered the field of view without body rotation, the OF PD controller generated yaw accelerations in the correct direction, steering the body towards the target (figure 11*b*). Yaw acceleration increased with larger OTA (x^g_{bee} and $|y^g_{bee}|$), indicating a stronger initial steering response. Thus, even before active body rotation, the OF PD controller alone provides the initial yaw steering necessary to reduce OTA and stabilize gaze.

4. Discussion

Our study provides new insights into how bumblebees integrate visual and inertial cues to land on laterally oscillating targets. Using high-speed kinematic tracking and control-theoretic modelling, we identified feedback structures underlying precise

Downloaded from royalsocietypublishing.org/rsif/article-pdf/doi/10.1098/rsif.2025.1198/6167060/rsif.2025.1198.pdf
by guest
on 30 September 2026

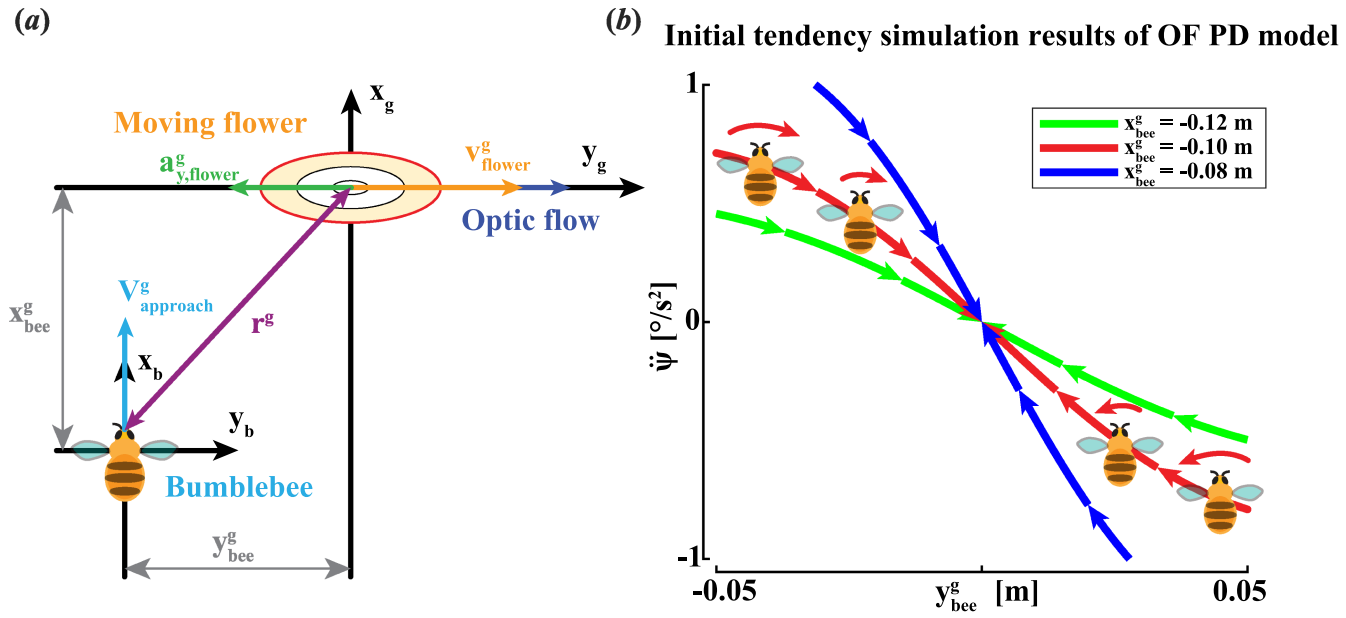


Figure 11. Flying bumblebees use OF-based yaw control to land on a moving flower. (*a*) Simulation set-up with the OF PD model for gaze control. The bumblebee flies forward at $|V^g_{approach}| = 2.1$ cm s^{-1} from positions $x^g_{bee} = [-0.012, -0.010, -0.008]$ m and $y^g_{bee} = [-0.05, 0.05]$ m. The flower moves sideways at $|v^g_{flower}| = 0.16$ m s^{-1} with acceleration $a^g_{y,flower} = -1.97$ m s^{-2}. Yaw acceleration is estimated for each condition using the PD model. (*b*) Instantaneous yaw acceleration (ordinate) for combinations of y^g_{bee} (abscissa) and x^g_{bee} (colour-coded). Bees consistently rotate towards the target, with stronger yaw acceleration at larger sideways offsets ($|y^g_{bee}|$) and shorter distances (x^g_{bee}).

tracking and gaze stabilization. The following sections place these findings within existing insect flight control research and discuss implications for multi-modal sensory integration.

4.1. Proportional and proportional–differential models for landing control

Originating from control theory, PID models are widely applied to describe insect flight behaviours for their simplicity, interpretability and ability to capture core feedback dynamics. In insect flight studies, such models approximate neural feedback loops and offer insight into how sensory inputs are transformed into motor commands [14,19,20,24,26,27]. P models have quantified visual speed control in fruitflies (*Drosophila*) [19], PD models describe speed regulation integrating visual and antennal feedback [14] and PI models capture attitude stabilization during perturbations where haltere-sensed angular rates drive corrective aerodynamic torques [24,26,27].

Consistent with these studies, our results show that a simple P model accurately describes sideways-movement control during bumblebee landings. Adding derivative or integral terms did not improve, and sometimes degraded, model performance. From a control-theoretic perspective, this is expected: the integral term mainly removes steady-state error, whereas proportional and derivative terms respond to instantaneous error and its future trend. In previous work on fruitflies [24,26,27], PI or PD models were appropriate because the task involved restoring a steady state after perturbation. By contrast, our landing scenario involves a continuously oscillating target whose desired state changes rapidly. Under such conditions, proportional control is sufficient for lateral tracking, prioritizing responsiveness over eliminating small steady-state errors.

By contrast, gaze control required a PD structure, highlighting a fundamental difference between translational and rotational control. Maintaining gaze on a moving target is highly dynamic and benefits from derivative feedback, which anticipates OF changes and adjusts yaw acceleration. This predictive component is particularly important at high-frequency oscillations, where proportional control alone would introduce phase lag and compromise visual alignment. The derivative term therefore acts as a damping component, reducing overshoot and improving transient response, consistent with control strategies reported in other insects during rapid rotational manoeuvres [20,24]. The similar sensory–motor delays estimated for both controllers suggest that these feedback loops may operate in parallel, possibly sharing neural pathways but tuned differently for translational and rotational control.

4.2. Optic-flow plays an important role in bumblebee flight control

To control flight and landing, bumblebees rely on compound eyes with a large field of view [4], enabling sensitivity to OF generated by the relative motion of the surroundings [37]. Previous studies show that optic-expansion guides approach and landing on stationary targets [3,5], while OF supports navigation and collision avoidance [8,38]. Our results are consistent with this body of work: model fitting indicates that OF plays a prominent role in both sideways movement and gaze control. Simulations further

Downloaded from royalsocietypublishing.org/rsif/article-pdf/doi/10.1098/rsif.2025.1198/6167060/rsif.2025.1198.pdf
by guest
on 30 September 2026

suggest that bumblebees potentially integrate OF with yaw-rate feedback to estimate sideways motion relative to the flower-mimic in the inertial frame.

Contrary to previous reports suggesting that bees use OTA for gaze control when landing on moving flowers [1,6], our results indicate that OTA contributes little to gaze regulation under the present conditions. Pathway analysis showed that proportional and derivative OF pathways account for most of the model output, suggesting that steering towards moving targets is primarily driven by visual velocity cues rather than retinal position. Such velocity-dominated control is consistent with findings in fruitflies, where apparent positional centring emerges from motion-selective pathways and high-gain optomotor feedback [10,11], and object-tracking turns are coordinated through integrated motion cues rather than instantaneous retinal position [12]. Our simulations support this interpretation: even before body rotation begins, the OF PD controller generates yaw steering in the correct direction, with stronger responses at larger OTA, indicating intrinsic static stability without explicit position feedback.

The flower motion in our experiments was intentionally simplified. In natural environments, where floral motion is irregular and gust-driven, OTA may play a larger role in regulating sideways movement and gaze. Future robotic experiments could test the robustness of the proposed target-angle-free control model under more complex motion conditions.

4.3. Bumblebees potentially possess inertial sensory feedback

Previous studies of bee flight dynamics have primarily focused on visual sensory feedback [1,3,5,6,8,38]. Our model-fitting results, however, indicate that angular-rate feedback also contributes to bumblebee flight control. Unlike dipterans, which measure angular rates using halteres [16], bumblebees lack such specialized organs. Nevertheless, two mechanisms could provide angular-rate estimates during flight [15,17,18]. First, mechanosensory feedback from campaniform sensilla on the wings can encode rotational strain, as shown in hawkmoths [15,17]. Second, angular rates could be inferred visually from OF patterns using established computational approaches [18]. Future experiments are needed to determine which mechanism bumblebees employ.

4.4. Comparison of sensory delay for controlling sideways movements and yaw rotations

The sensory–motor delay of honeybees tracking low-frequency moving targets has been estimated at under 80 ms [6]. Our results corroborate this finding: model fitting yielded effective closed-loop delays of $\tau_{sideway} = 54.00$ [52.05–56.08] ms and $\tau_{gaze} = 52.02$ [51.13–52.72] ms for sideways tracking and gaze control under the tested conditions (2 Hz flower oscillation and 2.5 cm amplitude). These delays did not differ significantly (paired *t*-test, $p = 0.33$), suggesting tight coupling between yaw and roll control, possibly involving shared or neighbouring neural pathways.

Bumblebees in our experiments also showed shorter delays than hawkmoths performing similar tracking tasks (approx. 60 ms) [28] and fruitflies controlling flight speed visually (approx. 100 ms) [14]. For body attitude regulation, the delays observed here (approx. 52 ms) are comparable to those reported for fruitflies during yaw correction manoeuvres (approx. 45 ms) [24]. While these comparisons indicate that the estimated delays are biologically plausible, differences in task structure, stimulus dynamics and modelling approaches may influence the reported values.

4.5. Study limitations and future directions

Several limitations of this study should be acknowledged. First, experiments were conducted under a single stimulus condition, with the flower-mimic oscillating laterally at 2 Hz and 2.5 cm amplitude. The estimated delays should therefore be interpreted as condition-specific rather than general sensorimotor delays for bumblebee flight control. Because sensorimotor delays depend on stimulus dynamics and task demands, future experiments varying target frequency and amplitude could reveal how control strategies and response delays adapt across dynamic regimes and whether predictive mechanisms emerge under periodic stimulation. Second, OF in this study was defined using a simplified geometric formulation based on the relative lateral motion between the bee and the flower-mimic. While this formulation captures the dominant visual cue for lateral tracking under the present conditions, it represents only a reduced component of the full retinal OF field and does not account for its natural spatio-temporal complexity. Third, the control models were intentionally minimal and phenomenological, identifying behaviourally sufficient feedback structures rather than the underlying neural implementation. Finally, the estimated delay represents an effective closed-loop delay between model inputs and behavioural outputs, reflecting the combined effects of sensory processing, motor actuation, body dynamics and aerodynamic force generation. It should therefore not be interpreted as a pure sensory or neural processing delay. Future work separating modality-specific delays and combining behavioural experiments with neurophysiological approaches could further clarify the neural mechanisms underlying visuomotor coordination in insect flight.

5. Conclusion

Our study shows that the sideways flight control of bumblebees landing on a moving target can be captured by a modular feedback control architecture (figure 12*a*). Observed behaviours are consistent with the integration of visual (OF) and angular-rate (yaw-rate) cues in regulating lateral motion and yaw kinematics. Sideways tracking is well described with proportional control based on OF and yaw rate, while yaw-based gaze stabilization follows a PD scheme using the same inputs. Under the experiment condition, both loops operate with similar effective closed-loop delays (approx. 54 ms and approx. 52 ms (figure 12*b*)), and lateral

Downloaded from royalsocietypublishing.org/rsif/article-pdf/doi/10.1098/rsif.2025.1198/6167060/rsif.2025.1198.pdf
by guest
on 30 September 2026

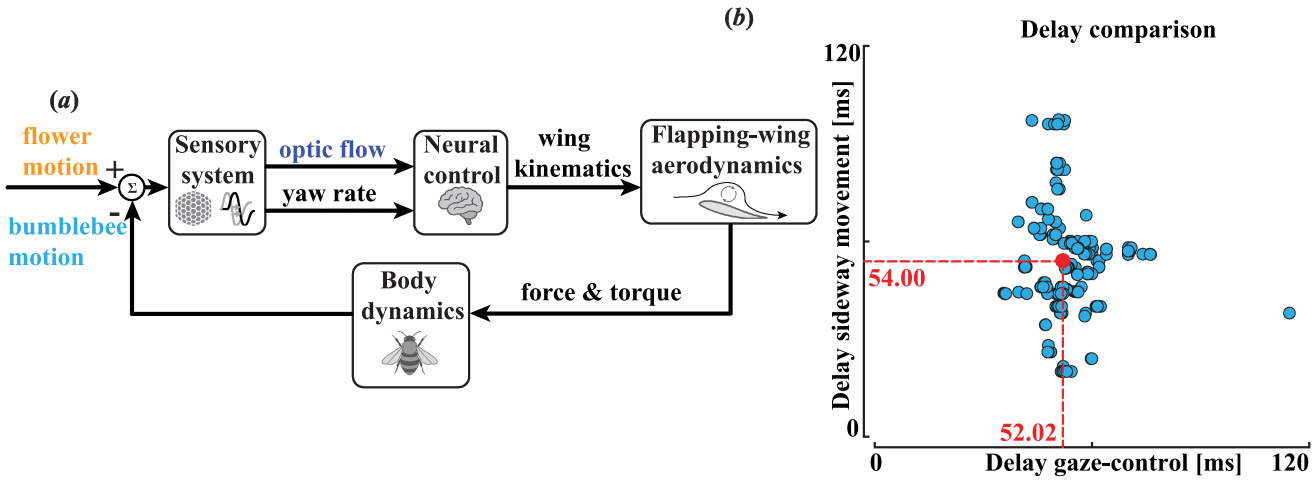


Figure 12. Closed-loop sensory–motor control model for bumblebees landing on a moving flower. (*a*) Diagram of the complete control loop, including sensory input, neural controller and motor output. (*b*) Comparison of case-specific effective sensory–motor delays for sideways-movement and gaze control across 48 landings; nearly identical median values are highlighted in red.

accelerations correlate strongly with body roll, consistent with the helicopter model of aerodynamic force vectoring. An intriguing outcome of this study is the negligible role of OTA in gaze control, despite its presumed importance in earlier work. This suggests that bumblebees prioritize velocity-based cues over position-based cues when tracking rapidly oscillating targets, a strategy that may enhance robustness under dynamic conditions. These findings deepen our understanding of multi-modal flight control and provide bio-inspired principles for agile UAV design.

Ethics. This work did not require ethical approval from a human subject or animal welfare committee.

Data accessibility. The data and code supporting this study are publicly available from the Dryad Digital Repository at [39]. Supplementary material is available online [40].

Declaration of AI use. AI-assisted technologies were used only for text revision and creating figure icons in this article. No original data or figures were generated by AI.

Authors' contributions. C.W.: formal analysis, investigation, methodology, software, validation, visualization, writing—original draft; L.J.d.V.: conceptualization, methodology, resources, writing—review and editing; V.v.d.P.: conceptualization, investigation, methodology, writing—review and editing; S.W.: investigation, supervision, writing—review and editing; C.D.W.: investigation, supervision, writing—review and editing; F.T.M.: conceptualization, data curation, funding acquisition, investigation, methodology, project administration, resources, supervision, writing—review and editing.

All authors gave final approval for publication and agreed to be held accountable for the work performed therein.

Conflict of interest declaration. We declare we have no competing interests.

Funding. This research was supported by an NWO Vidi grant (VI.Vidi.193.054) awarded to F.T.M.

Acknowledgements. We thank Dapeng Sun, Remco Pieters, Henk Schipper and Leonardo Honfi Camilo for assistance with the experiments and analyses. We thank Remco Huvermann from Koppert BV for providing the bumblebee colony.

References

1. de Vries LJ, van Langevelde F, van Leeuwen JL, Naguib M, Pieters RPM, Muijres FT. 2025 Follow the flower: approach-flight behaviour of bumblebees landing on a moving target. *J. Exp. Biol.* **228**, jeb249380. (doi:10.1242/jeb.249380)
2. Baird E, Boeddeker N, Srinivasan MV. 2021 The effect of optic flow cues on honeybee flight control in wind. *Proc. R. Soc. B* **288**, 20203051. (doi:10.1098/rspb.2020.305)
3. Baird E, Boeddeker N, Ibbotson MR, Srinivasan MV. 2013 A universal strategy for visually guided landing. *Proc. Natl Acad. Sci. USA* **110**, 18 686–18 691. (doi:10.1073/pnas.1314311110)
4. Egelhaaf M. 2023 Optic flow based spatial vision in insects. *J. Comp. Physiol. A* **209**, 541–561. (doi:10.1007/s00359-022-01610-w)
5. Goyal P, Cribellier A, de Croon GCHE, Lankheet MJ, van Leeuwen JL, Pieters RPM, Muijres FT. 2021 Bumblebees land rapidly and robustly using a sophisticated modular flight control strategy. *iScience* **24**, 102467. (doi:10.1016/j.isci.2021.102407)
6. Zhang SW, Xiang W, Zili L, Srinivasan MV. 1990 Visual tracking of moving targets by freely flying honeybees. *Vis. Neurosci.* **4**, 379–386. (doi:10.1017/s0952523800004582)
7. Gibson JJ. 1950 *The perception of the visual world*, 1st edn. Boston, MA: Houghton Mifflin.
8. Baird E, Srinivasan MV, Zhang S, Cowling A. 2005 Visual control of flight speed in honeybees. *J. Exp. Biol.* **208**, 3895–3905. (doi:10.1242/jeb.01818)
9. de Croon GCHE. 2016 Monocular distance estimation with optical flow maneuvers and efference copies: a stability-based strategy. *Bioinspir. Biomim.* **11**, 016004. (doi:10.1088/1748-3190/11/1/016004)
10. Fenk LM, Kim AJ, Maimon G. 2021 Suppression of motion vision during course-changing, but not course-stabilizing, navigational turns. *Curr. Biol.* **31**, 4608–4619. (doi:10.1016/j.cub.2021.09.068)
11. Rimniceanu M, Limbania D, Wasserman SM, Frye MA. 2024 Divergent visual ecology of *Drosophila* species drives object-tracking strategies matched to landscape sparsity. *Curr. Biol.* **34**, 4743–4755. (doi:10.1016/j.cub.2024.08.036)

Downloaded from royalsocietypublishing.org/rsif/article-pdf/doi/10.1098/rsif.2025.1198/6167060/rsif.2025.1198.pdf
by guest
on 30 September 2026

12. Mongeau JM, Frye MA. 2017 *Drosophila* spatiotemporally integrates visual signals to control saccades. *Curr. Biol.* **27**, 2901–2914. (doi:10.1016/j.cub.2017.08.035)
13. Goyal P, van Leeuwen JL, Muijres FT. 2024 Bumblebees compensate for the adverse effects of sidewind during visually guided landings. *J. Exp. Biol.* **227**, jeb246106. (doi:10.1101/2022.12.16.520721)
14. Fuller SB, Straw AD, Peek MY, Murray RM, Dickinson MH. 2014 Flying *Drosophila* stabilize their vision-based velocity controller by sensing wind with their antennae. *Proc. Natl Acad. Sci. USA* **111**, E1182–E1191. (doi:10.1073/pnas.1323529111)
15. Dickerson BH, Aldworth ZN, Daniel TL. 2014 Control of moth flight posture is mediated by wing mechanosensory feedback. *J. Exp. Biol.* **217**, 2301–2308. (doi:10.1242/jeb.103770)
16. Pringle JWS. 1948 The gyroscopic mechanism of the halteres of Diptera. *Phil. Trans. R. Soc. B* **233**, 347–384. (doi:10.1098/rstb.1948.0007)
17. Eberle AL, Dickerson BH, Reinhall PG, Daniel TL. 2015 A new twist on gyroscopic sensing: body rotations lead to torsion in flapping, flexing insect wings. *J. R. Soc. Interface* **12**, 20141088. (doi:10.1098/rsif.2014.1088)
18. Longuet-Higgins HC, Prazdny K. 1980 The interpretation of a moving retinal image. *Proc. R. Soc. B* **208**, 385–397. (doi:10.1098/rspb.1980.0057)
19. Rohrseitz N, Fry SN. 2011 Behavioural system identification of visual flight speed control in *Drosophila melanogaster*. *J. R. Soc. Interface* **8**, 171–185. (doi:10.1098/rsif.2010.0225)
20. Cellini B, Salem W, Mongeau J-M. 2022 Complementary feedback control enables effective gaze stabilization in animals. *Proc. Natl Acad. Sci. USA* **119**, e2121660119. (doi:10.1073/pnas.2121660119)
21. Cai X, Liu H. 2021 A six-degree-of-freedom proportional-derivative control strategy for bumblebee flight stabilization. *J. Biomech. Sci. Eng.* **16**, 21-00113. (doi:10.1299/jbse.21-00113)
22. Wang C, Wang S, De Croon G, Hamaza S. 2022 Embodied airflow sensing for improved in-gust flight of flapping wing MAVs. *Front. Robot. AI* **9**, 1060933. (doi:10.3389/frobt.2022.1060933)
23. Dickson W, Straw A, Poelma C, Dickinson M. 2006 An integrative model of insect flight control. In *44th AIAA Aerospace Sciences Meeting and Exhibit*. Reston, VA: AIAA. (doi:10.2514/6.2006-34)
24. Ristroph L, Bergou AJ, Ristroph G, Coumes K, Berman GJ, Guckenheimer J, Wang ZJ, Cohen I. 2010 Discovering the flight autostabilizer of fruit flies by inducing aerial stumbles. *Proc. Natl Acad. Sci. USA* **107**, 4820–4824. (doi:10.1073/pnas.1000615107)
25. Cheng B, Deng X. 2011 Translational and rotational damping of flapping flight and its dynamics and stability at hovering. *IEEE Trans. Robot.* **27**, 849–864. (doi:10.1109/TRO.2011.2156170)
26. Whitehead SC, Beatus T, Canale L, Cohen I. 2015 Pitch perfect: how fruit flies control their body pitch angle. *J. Exp. Biol.* **218**, 3508–3519. (doi:10.1242/jeb.122622)
27. Beatus T, Guckenheimer JM, Cohen I. 2015 Controlling roll perturbations in fruit flies. *J. R. Soc. Interface* **12**, 20150075. (doi:10.1098/rsif.2015.0075)
28. Sponberg S, Dyhr JP, Hall RW, Daniel TL. 2015 Luminance-dependent visual processing enables moth flight in low light. *Science* **348**, 1245–1248. (doi:10.1126/science.aaa3042)
29. Åström KJ, Murray RM. 2021 *Feedback systems: an introduction for scientists and engineers*, 2nd edn. Princeton, NJ: Princeton University Press.
30. Sane SP, Jacobson NP. 2006 Induced airflow in flying insects I. A theoretical model of the induced flow. *J. Exp. Biol.* **209**, 32–42. (doi:10.1242/jeb.01957)
31. Mathis A, Mamidanna P, Cury KM, Abe T, Murthy VN, Mathis MW, Bethge M. 2018 DeepLabCut: markerless pose estimation of user-defined body parts with deep learning. *Nat. Neurosci.* **21**, 1281–1289. (doi:10.1038/s41593-018-0209-y)
32. Theriault DH, Fuller NW, Jackson BE, Bluhm E, Evangelista D, Wu Z, Betke M, Hedrick TL. 2014 A protocol and calibration method for accurate multi-camera field videography. *J. Exp. Biol.* **217**, 1843–1848. (doi:10.1242/jeb.100529)
33. Cribellier A, Buchner A-J. 2024 A Python package to track the 3D flight kinematic of insects with DeepLabCut. In *SEB Conf. Prague 2024, Prague, Czech Republic, 2–5 July 2024*.
34. Koenderink JJ. 1986 Optic flow. *Vision. Res.* **26**, 161–179. (doi:10.1016/0042-6989(86)90078-7)
35. Muijres FT, Elzinga MJ, Melis JM, Dickinson MH. 2014 Flies evade looming targets by executing rapid visually directed banked turns. *Science* **344**, 172–177. (doi:10.1126/science.1248955)
36. Warfvinge K, Johansson LC, Hedenström A. 2021 Hovering flight in hummingbird hawkmoths: kinematics, wake dynamics and aerodynamic power. *J. Exp. Biol.* **224**, jeb230920. (doi:10.1242/jeb.230920)
37. Dyhr JP, Higgins CM. 2010 The spatial frequency tuning of optic-flow-dependent behaviors in the bumblebee *Bombus impatiens*. *J. Exp. Biol.* **213**, 1643–1650. (doi:10.1242/jeb.041426)
38. Baird E, Kornfeldt T, Dacke M. 2010 Minimum viewing angle for visually guided ground speed control in bumblebees. *J. Exp. Biol.* **213**, 1625–1632. (doi:10.1242/jeb.038802)
39. Wang C, de Vries LJ, van de Pas V *et al*. 2026 Data and code from: Visual-inertial integration enables bumblebees to land on rapidly moving flowers [Dataset]. Dryad. (doi:10.5061/dryad.37pvmcvzz)
40. Wang C, de Vries LJ, van de Pas V, Werner S, De Wagter C, Muijres FT. 2026 Supplementary material from: Visual-inertial integration enables bumblebees to land on rapidly moving flowers. Figshare. (doi:10.6084/m9.figshare.c.8583027)

Downloaded from royalsocietypublishing.org/rsif/article-pdf/doi/10.1098/rsif.2025.1198/6167060/rsif.2025.1198.pdf
by guest
on 30 September 2026